Available online at www.sciencedirect.com
SCIENCE DIRECT®
Journal of Nuclear Materials 323 (2003) 169–180
journal of nuclear materials
www.elsevier.com/locate/jnucmat

Modeling the microstructural evolution in bcc-Fe during irradiation using kinetic Monte Carlo computer simulation

N. Soneda [a,*], S. Ishino [a,b], A. Takahashi [c], K. Dohi [a]

[a] *Department of Materials Science, Komae Research Laboratory, Central Research Institute of Electric Power Industry, 2-11-1 Iwado-kita, Komae-shi, Tokyo 201-8511, Japan*

[b] *Department of Applied Science, Tokai University, 1117 Kitakaname, Hiratsuka, Kanagawa 259-1292, Japan*

[c] *Department of Quantum Engineering and System Science, The University of Tokyo, 7-3-1 Hongo, Bunkyo-ku, Tokyo 113-8656, Japan*

Abstract

Kinetic Monte Carlo (KMC) simulations of defect accumulation in neutron-irradiated bcc-Fe are presented. Comparisons of the KMC simulations with the recent experimentals are made to discuss the validity of the proposed KMC model. Then, the effect of environmental variables such as irradiation temperature, dose rate, and neutron spectrum is studied using the technique. The magnitude of dose rate effect is irradiation-temperature dependent, and it is found that a threshold dose rate, below which defect accumulation is not affected by the difference of dose rate, exists when irradiated at 600 K. An evaluation of the number of vacancy jumps of both irradiation-induced vacancies as well as thermal vacancies is done to study a possible effect of dose rate on a solute diffusion in bcc-Fe. The results show that the total number of vacancy jumps is dose rate dependent at very low and high dose rates while there is a dose rate independent region in between.

PACS: 02.70.Lq; 61.72.Cc; 61.80.Az; 61.80.Hg

1. Introduction

Understanding the fundamental mechanisms of microstructure evolution in steels under neutron irradiation is very important for the safe operation of reactor pressure vessels of aged light water reactors [1] and for the design of future fusion reactor components. In the real steels, it is well known that some of the key solute elements control the response of the materials to the neutron irradiation, and the behavior of such elements is often of the primary concern. Nevertheless, the knowledge on the microstructure evolution in pure bcc-Fe is still very informative. A clear picture of defect production in pure bcc-Fe will enhance the understandings of the effects of solute elements on defect production in alloys. Furthermore, knowledge of the vacancy behavior in pure Fe under different irradiation conditions is essential to understand the behavior of substitutional solute atoms that diffuse by vacancy mechanism.

A large body of experimental works on the fundamental properties of point defects in bcc-Fe and the defect accumulation in bcc-Fe under electron [2], ion [3], and neutron irradiations [4] has been compiled to date. However, we still do not have a comprehensive model that can describe the response of bcc-Fe to different irradiation conditions. One example that requires such a model is the effect of dose rate on the embrittlement of the reactor pressure vessel materials. The effect of dose rate on microstructure evolution in bcc-Fe is very important issue for the reactor pressure vessel materials because the experiments at the higher dose rates can never imitate the real behavior of the materials in the operating reactors. Development of a predictive model that can identify the controlling process is inevitable to address this kind of issues.

* Corresponding author. Tel.: +81-3 3480 2111; fax: +81-3 3430 2410.
E-mail address: soneda@criepi.denken.or.jp (N. Soneda).

0022-3115/$ - see front matter © 2003 Elsevier B.V. All rights reserved.
doi:10.1016/j.jnucmat.2003.08.021

One promising approach is the utilization of the atomistic-scale computer simulation techniques that have achieved great progress over the last decade in providing information that are hardly detected or measured by currently available experimental techniques [5,6]. Among the techniques, a kinetic Monte Carlo (KMC) computer simulation method combined with the database developed by molecular dynamics (MD) simulations is a technique that allows us to simulate the defect behavior and the microstructure evolution in materials under irradiation [7–10]. KMC utilizes all the detailed information on defect production by displacement cascades, diffusion of point defects, and clustering and dissociation of defect clusters to simulate the materials behavior over large time and length scales. The objective of our study is to perform KMC simulations of irradiated bcc-Fe to identify the mechanisms that can contribute to the microstructure changes.

In this paper, we summarize the model that we use in our KMC simulations. A new numerical method is proposed to take the effect of grain boundaries in consideration under the framework of the conventional periodic boundary condition. The validity of the present approach is verified through comparisons between simulation results and available experimental data on irradiated bcc-Fe. Then we present KMC simulation results focusing on the effects of irradiation temperature, dose rate, and neutron spectrum. Finally, results on the number of vacancy jumps, which can be a measure of solute diffusion in irradiated bcc-Fe, and the effect of defect sinks on point defect annihilation are discussed.

2. Computer simulation

2.1. Kinetic Monte Carlo simulation

KMC calculates defect accumulation by simulating all the possible events, such as displacement cascades, diffusion of point defects and defect clusters, and dissociation of defect clusters, that can happen in the computation crystal. At the beginning of each KMC time step, the occurrence frequencies (or probabilities) of all the events are calculated and summed up to obtain a total frequency, P. Then a uniform random number, R, whose value ranges from zero to the total frequency is generated to pick up one event that is to occur at the time step. The elapsed time for the picked-up event, Δt, is calculated by $\Delta t = -\log(R*P)/P$. After the picked-up event is done, if the crystal contains any two particles that are located within the interaction volume, then clustering or recombination of the two particles takes place. This process repeats until a given value of time or dose is reached. More details are explained elsewhere [9].

A periodic boundary condition has been commonly applied in the KMC simulations, where the effect of grain boundaries has never been considered. However, the grain boundaries are the places of interest for the defect accumulation simulations under irradiation because they are large sinks of point defects and also are the places for solute atoms to segregate. In this study, we propose a new periodic boundary condition, which can simulate a finite volume of a crystal grain. The idea of this new condition, *finite periodic boundary condition* (FPBC), is schematically shown in Fig. 1, where only x direction is considered for simplicity. Let us assume that we have n particles in the computation cell (box). The cell repeats infinitely when we apply the conventional periodic boundary condition. In the FPBC, however, we assume that the cell repeats a finite number, N, in x direction to simulate a given finite volume of a grain, and we also assume that each particle in the computation cell has its *home* cell out of the N imaginary cells. Assignment of the home cell to the particles is done randomly so that the average number of the particles that have the same home cell becomes n/N. Of course the particles interact with other particles even if their home cells are different. The idea of the home cell is applied only when particles cross the cell boundaries. If a particle, whose home cell is the ith cell, jumps over the cell boundary toward the left hand direction, then the home cell of the particle becomes the $(i-1)$th cell. If a particle in the first cell jumps toward the left hand direction, then we assume that the particle hits a grain boundary. If the particle is a point defect or a point defect cluster, then we remove the particle from the computation box to simulate the annihilation at the grain boundary. It should be noted that all the cells in the FPBC are basically equivalent except for the cells adjacent to the grain boundary. In the following simulations, the size of the computation cell is $100\times100\times100$ mm^3, and the number of the cells is determined according to the grain size assumed.

Another feature that needs to be considered is a pre-existing dislocation. In the current KMC code, the CPU cost to handle one-dimensional features of dislocations is very expensive, so we introduce point sinks as replacements of one-dimensional dislocations. We determine the number of point sinks so that the sum of the interaction volume of the point sinks becomes almost equivalent to that of the one-dimensional dislocations of assumed dislocation density. We place 1000 point sinks in a cell in this study.

We developed a new KMC code in the present work. The code basically follows the algorithm of the *bigmac* code [9]. The difference between the codes is that no event table is used in our new code in order to save the required computer memory. The idea of the event table in the *bigmac* code allows us a large flexibility in handling different types of crystals, defects and impurities. However, when we simulate defect accumulation to high doses, the table sometimes becomes very large according

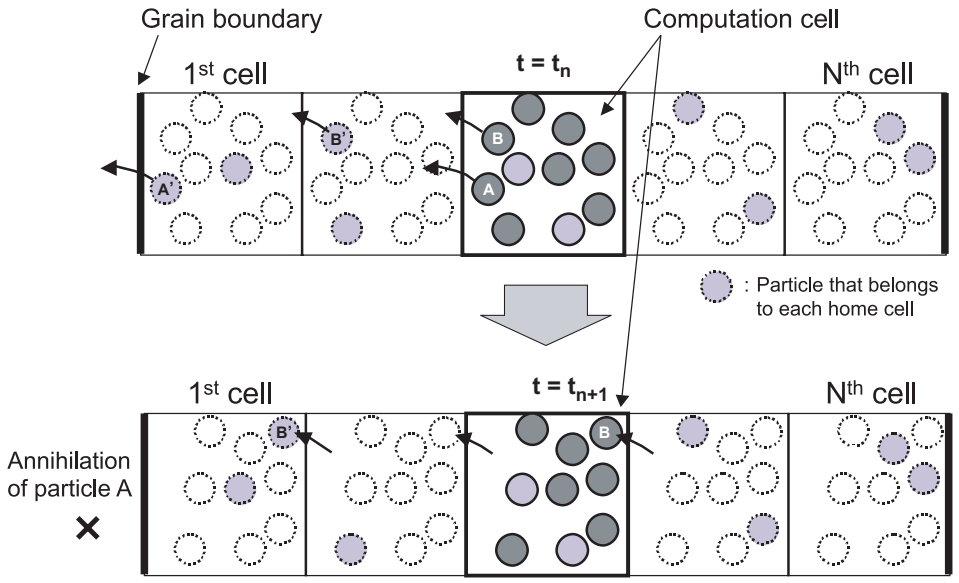

Fig. 1. Concept of *finite periodic boundary condition*. A conventional periodic boundary condition is applied to particle 'B' so that it comes back from the opposite side of the computation cell. However, when particle 'A', whose home cell is adjacent to a grain boundary, crosses over the grain boundary, it is removed from the computation cell at the jump.

to the increase of the maximum size of defect clusters. This results in a huge required computer memory, which makes simulations very difficult to be performed. Our new code calculates reaction properties anytime when it is requested rather than storing those properties on memory.

2.2. Data set on defect production and defect kinetics

The KMC simulations require detailed information on the defect production due to displacement cascades with different primary knock-on atom (PKA) energies, diffusivities and diffusion modes of point defects and defect clusters, and the binding energies of defect clusters.

Information on the defect production due to displacement cascades is obtained by performing extensive MD simulations. We have compiled a database of displacement cascades for the PKA energies of 100, 200, 500 eV, 1, 2, 5, 10, 20 and 50 keV at 600 K in order to simulate arbitrary PKA energy spectra due to different irradiation conditions [10–12]. Less than 10 simulations with randomly selected different knock-on directions were performed for each of the PKA energies less than 20 keV because the difference in defect production among the results at these low PKA energies is not very large. At the PKA energies greater than 20 keV, however, sub-cascade formation gives rise to the diversity in defect production, and this is further enhanced at 50 keV PKA energy. Therefore, in order to obtain better statistics, we have performed 50 and 100 simulations for 20 and 50 keV PKA energies, respectively, using random knock-on directions. Our general observations in the cascade database are (1) the chances for a large (more than 20 members) self-interstitial atom (SIA) cluster and a vacancy cluster to be formed are about 10% and 2%, respectively, in 20 keV cascades, while they are about 30% and 10% in 50 keV cascades, and (2) very large SIA clusters whose diameters are larger than 1 nm are directly formed in the displacement cascade event at the place where two adjacent sub-cascades overlap [11].

The PKA energy spectrum by fast neutron irradiation is simulated in the KMC simulations by the combination of the above cascade database. We used the PKA energy spectrum calculated by Greenwood [13] for fission neutrons. The mean PKA energy is 24 keV, and the fraction of PKAs with the energy greater than 20 keV is 56% in the fission spectrum used in the present study. At a fusion first wall, the neutron energy spectrum is softer than that for fission neutrons resulting in the increase of fraction of small mobile point defect clusters. This suggests that the diffusion of small point defects should be more important than in fission spectrum.

We also used MD to calculate the diffusivities and diffusion modes of point defects and defect clusters, and the binding energies of defect clusters. The detailed values of these properties can be found elsewhere [10,14]. In the KMC simulations, we assumed that mono-, di- and tri-SIA clusters diffuse in the mode of the combination of one-dimensional motion in $\langle 1\,1\,1\rangle$ direction and rotation. For 4- to 20-member SIA clusters, only

one-dimensional motion is applied. The other larger SIA clusters are assumed to be sessile. MD simulations show that SIA clusters larger than 20 in size are still mobile in bcc-Fe [15,16]. However, it is also true that the mobility of such SIA clusters is reduced by several reasons [6]. Trapping by impurity element is one of the possibilities. The assumption of sessile large SIA cluster effectively considers such possibilities. Dissociation of a cluster occurs by emitting one cluster member with an activation energy of the sum of the binding energy and the migration energy of the diffusing particle. The migration energy of a single vacancy obtained by MD is about 0.87 eV [10] while the experimental value of ultra high purity Fe is 0.5 eV [17]. This difference is not trivial, and we used the experimental value of 0.5 eV in the KMC simulations.

When two particles meet within their reaction volume, they transform to a new particle. We assumed an isotropic spherical reaction volume for all the possible particles. The radius of the recombination volume is that of a sphere with the same volume as the particle [9]. The actual recombination radius (distance) is a sum of the recombination radii of the two particles added by an offset of a lattice constant. When one or two of the particles are of SIA type, this offset value is increased by 15% in order to effectively consider the larger strain field of the SIA clusters than vacancy clusters. The reaction of the two particles of the same kind is a growth of that kind of particle. However, our MD simulations show that the reaction of a SIA cluster and a vacancy cluster is a little bit complex. When the two particles make a head-on collision, then the smaller cluster completely annihilates leaving the larger particle whose size is decreased by that of the smaller particle. On the other hand, when the two particles make an offset collision, only a small part of each particle annihilates leaving the remaining part of the particles unaffected [18]. In this study, however, we assumed that if two particles of different kinds come in the recombination volume, the whole smaller cluster annihilates and the larger cluster shrinks. When a migrating defect cluster meets a dislocation, the particle is assumed to be absorbed at the dislocation. The radius of the recombination volume for a point sink dislocation is assumed to be 1.5 times the lattice constant.

3. Results and discussion

3.1. Comparisons with experimental data

We first compare the KMC results obtained using our model for bcc-Fe with the recent experimental data in order to see how our model describes experimental observations. Fig. 2 shows the comparison with the data obtained by Eldrup et al. [19]. The calculated number density of vacancy clusters counts all the vacancy clusters no matter what their sizes are, while the calculated number densities of SIA clusters counts only those clusters containing more than 37- and 100-SIAs. KMC results for vacancy clusters agree very well with the experiment in terms of the absolute values as well as the slope of the curve at doses between 10^{-5}–10^{-3} dpa. At high doses, experimental data show a saturation tendency while no saturation is observed in the KMC results. One possible explanation for this discrepancy is that the number density measured by the positron annihilation spectroscopy (PAS) tends to saturate when the concentration of vacancies reaches a certain value. It is known that the response of PAS saturates if there are sufficient number of vacancies to trap all the positrons. The number density of the order of 10^{24} m^{-3} will be sufficiently high to trap all the positrons.

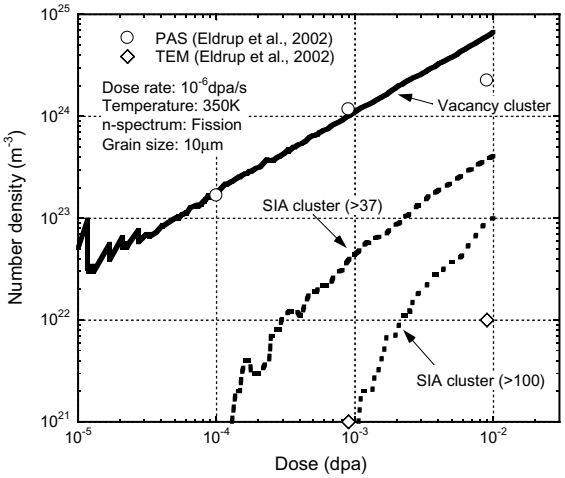

Fig. 2. Comparison of the KMC results with the experimental data obtained using PAS and TEM techniques by Eldrup et al. [19]. Broken and dotted lines show the number densities of the SIA clusters containing more than 37 and 100 SIAs, respectively.

Fig. 3 shows the calculated size distribution of vacancy clusters at different doses. The same type of plot from experiment is shown in the literature [19]. The calculated number densities of vacancy clusters for the mean size of 0.35 nm are smaller than those of experiments. Our view is that very small amount of impurity atoms such as carbon should exist even in pure Fe, and trapping of vacancies by such impurity atoms may affect the number density of the small vacancy clusters. In the current KMC simulation model, mono- and di-vacancies keep diffusing without being trapped and this will make the population of small vacancy clusters small. Regarding the large vacancy clusters, the formation of large vacancy clusters greater than 1 nm in diameter at high doses in experiments is well reproduced by the KMC simulations. We conclude that overall cluster size

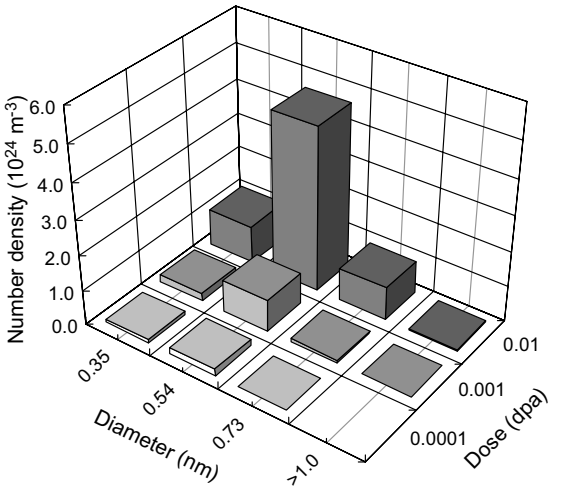

Fig. 3. Size distribution of vacancy clusters at different doses. The diameter, d, is calculated from the equation: $d = 2 \cdot \sqrt[3]{\frac{3n\Omega}{4\pi}}$, where n and Ω are number of vacancies in the vacancy cluster and the atomic volume, respective.

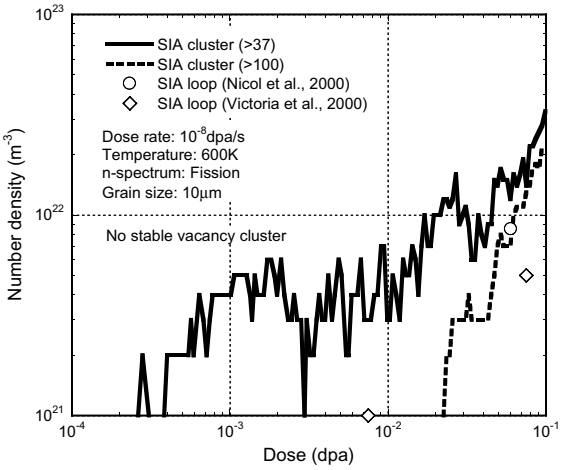

Fig. 4. Comparison of the KMC results with the experimental data obtained using TEM technique by Victoria et al. [21] and Nicol et al. [22]. The irradiation temperature is 600 K. No stable vacancy clusters are observed in the KMC at this temperature, in good correspondence to the experimental observations.

distribution also agree very well with the experimental results.

On the other hand for the SIA clusters, the number densities of the calculated SIA loops are larger than those measured by transmission electron microscopy (TEM). The size of the measured SIA loops is reported to be greater than 1 nm, and the diameters of 37 and 100 member SIA clusters are ~1.5 and ~2.5 nm, respectively. General tendency on the increase of the number density is very similar between the experiments and simulations. The simulation results for SIAs >100 members (~2.5 nm in diameter) are much closer to the experiments. There are a couple of factors that we need to consider when we compare the results. First, the number density of 10^{21} m^{-3} corresponds to one SIA loop in the computation cell. Therefore, there should be a non-trivial statistical uncertainty in the simulation results at low number densities. Second, we made a very simple assumption on the mobility of SIA loops: SIAs >20 members are sessile. This assumption implicitly considers the possibilities of loop trapping by impurities and the formation of such loops as $\langle 1\,0\,0\rangle$ loops. Of course this assumption needs to be improved in future, and more detailed and accurate understandings are necessary on the SIA loop formation and interactions. Third, there should also be uncertainties that inevitably arise in TEM experiments [20]. Considering these factors, we feel that our simulation captures the basic characteristics of the formation of SIA clusters.

Another comparison between experiments and KMC simulations is made in Fig. 4. In this comparison, irradiation temperature is increased from 350 K of Fig. 2 to 600 K, and the dose rate is decreased down to 10^{-8} dpa/s. We compare the simulation results with experimental results by Victoria et al. [21] and Nicol and Jenkins [22]. The number densities of SIA loops measured by TEM in these experiments are very similar to those of KMC simulations, but of course the discussions raised above needs to be considered. The size distribution of SIA clusters is shown in Fig. 5. The size of the SIA loops calculated primarily ranges from 1 to 7 nm in good agreement with the reported range from 2 to 6 nm [22]. It should be noted that, though the absolute value of the number density of SIA loops in Fig. 4 is more than one

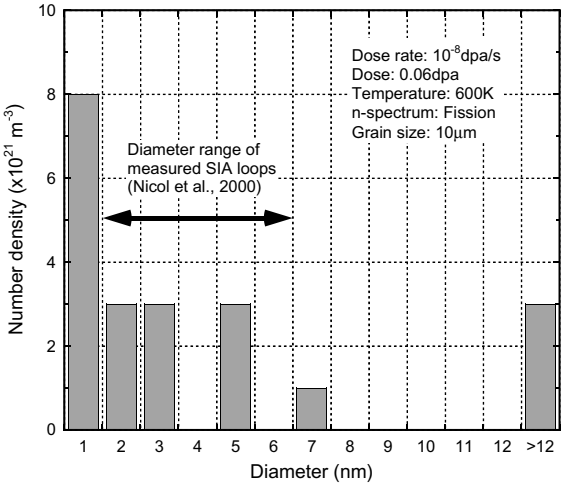

Fig. 5. Size distribution of SIA clusters. The diameters of the SIA clusters are calculated from the atomic arrangement of the $\frac{a_0}{2}\langle 111\rangle$ loop.

order of magnitude smaller than those in Fig. 2, KMC simulations reproduce these effect of the temperature and dose rate on the microstructure change well, demonstrating the validity of the KMC simulation model used in this study.

3.2. Effect of irradiation temperature, dose rate, and neutron spectrum

We then study using the KMC model the effects of three key irradiation variables: irradiation temperature, dose rate and neutron spectrum as a function of dose. Fig. 6 shows the effect of irradiation temperature at relatively high dose rate of 10^{-6} dpa/s. Solid and broken lines are the simulation results at 350 and 600 K, respectively. The effect of the irradiation temperature is significant especially at high doses, where the defect number densities at lower temperature irradiation are two orders of magnitude or more than those of the high temperature data. At low temperature irradiation, the slope of the solid line for vacancy clusters is almost unity suggesting that the vacancy number density is closely related to the dose or the number of displacement cascade events. However, at the higher temperature, the slope of the broken line for vacancy clusters is almost 1/2, which is much smaller than that at the lower temperature. The same discussions apply to SIA clusters. This will be discussed later.

The effect of dose rate in the range from 10^{-6} to 10^{-10} dpa/s at 350 K is shown in Fig. 7. The effect of dose rate is almost within a factor of 2 over the whole dose range. Even though the effect of dose rate is not very significant, we can see an overall tendency that the lower dose rate gives smaller defect densities. On the other hand, as one can see in Fig. 8(a) and (b), the effect of dose rate at the higher temperature is very large especially for the vacancy cluster formation. Fig. 8(a) shows the effect of dose rate on vacancy cluster formation. The number density of vacancy clusters at 10^{-4} dpa/s is more than one order of magnitude larger than that at 10^{-6} dpa/s. The slope is about 1/2 for the dose rates of 10^{-4} and 10^{-6} dpa/s. At lower dose rates of 10^{-8} and 10^{-10} dpa/s, no stable vacancy clusters were observed. Since the irradiation temperature of 600 K is the upper limit of stage V temperatures, almost all the vacancy clusters are thermally unstable at this temperature. Therefore, the vacancy clusters can exist only as meta-stable (or unstable) manner with continuous supply of vacancies that compensate the evaporation of vacancies from the vacancy clusters. At this condition, the formation process is basically nucleation and growth through free diffusion of vacancies rather than direct nucleation in cascades. It should be noted that the threshold dose rate to form unstable vacancy clusters lie between 10^{-8} and 10^{-6} dpa/s in the present results. Fig. 8(b) demonstrates the effect of dose rate on the SIA cluster formation. We can see clear dose rate effect at the dose rates from 10^{-4} to 10^{-8} dpa/s. However, the number density of the SIA cluster at 10^{-10} dpa/s is almost identical to that of 10^{-8} dpa/s, again suggesting a threshold dose rate to cause microstructure change. Of course this is closely related to the vacancy cluster formation in such a way that the formation of unstable vacancy clusters reduces the number of free vacancies to enhance the growth of SIA clusters.

Fig. 9(a) and (b) show the size distribution of the vacancy and SIA clusters, respectively, at different

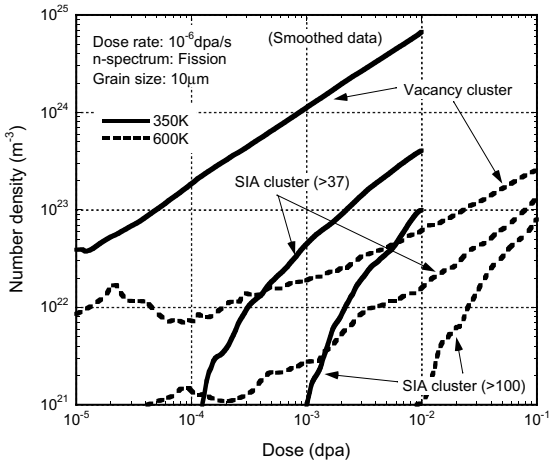

Fig. 6. Defect cluster formation at two different temperatures of 350 K (solid lines) and 600 K (broken lines). The lines are smoothed to reduce the fluctuation. Irradiation at the upper limit temperature of stage V (600 K) reduces the defect number density.

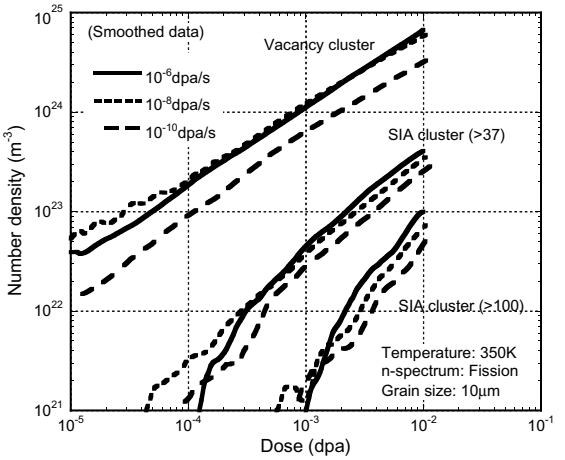

Fig. 7. Dose rate effect at the irradiation temperature of 350 K. Dose rate ranges from 10^{-10} to 10^{-6} dpa/s. Four orders of magnitude difference in dose rate do not affect very much on the defect number densities.

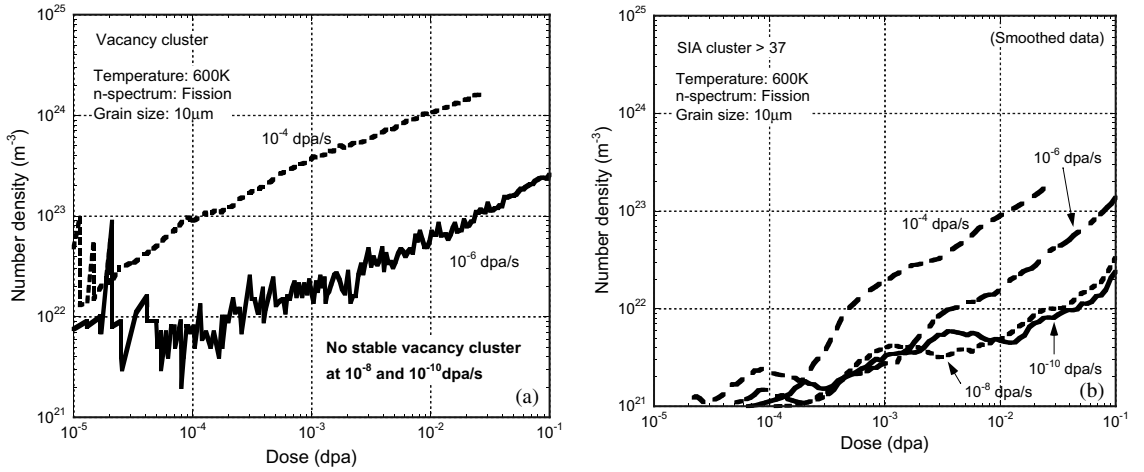

Fig. 8. Dose rate effect at the irradiation temperature of 600 K on (a) the vacancy cluster and (b) SIA cluster formation. (a) The lifetime of vacancy clusters is short at 600 K due to evaporation of vacancies from the clusters. Only high dose rate irradiation allows accumulation of the vacancy clusters. (b) The data of the SIA clusters are smoothed to clarify the difference of the lines at different dose rates. No difference is observed between the data at the dose rates of 10^{-8} and 10^{-10} dpa/s.

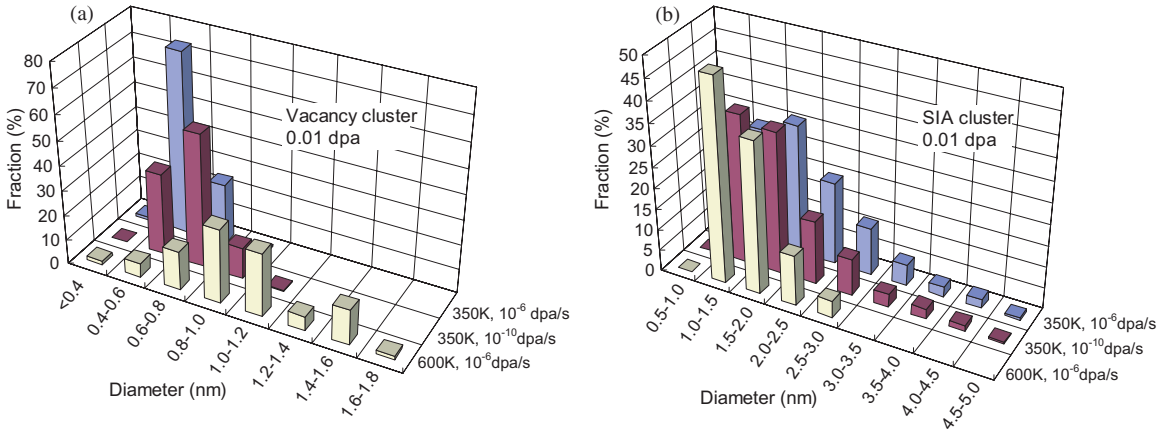

Fig. 9. Effects of dose rate and irradiation temperature on the size distribution of (a) vacancy clusters and (b) SIA clusters at 0.01 dpa.

temperatures and dose rates at the same dose of 0.01 dpa. The effect of dose rate on the number density of vacancy clusters at 350 K is not very large as we see in Fig. 7. However, we can see in Fig. 9(a) that the difference of dose rate at 350 K causes a clear difference in size distribution in such a way that the low dose rate enhance the growth of vacancy clusters. This tendency is largely enhanced at the higher temperature of 600 K, where there are very small amount of small vacancy clusters but large vacancy clusters, whose diameters are larger than 1 nm, are easily produced. The situation is consistently reversed for the size distribution of SIA clusters as can be seen in Fig. 9(b). The lower dose rate or the higher temperature suppresses the growth of SIA clusters.

The picture that explains these observations is as follows. Right after the cascade event, SIA clusters quickly diffuse to react with other particles before vacancies start to migrate. At the low temperature of 350 K, most of the vacancy clusters are thermally stable. So, what happens on vacancies is the annihilation by recombination with SIAs and/or formation of vacancy clusters. If dose rate is high, the fraction of clustering becomes larger resulting in the smaller size distribution of vacancy clusters. If dose rate is low, vacancies have sufficient time to diffuse resulting in the growth of vacancy clusters and the shrink of SIA clusters. In the cases of high temperature of 600 K, vacancy clusters are thermally unstable, and most of the small vacancy clusters evaporate immediately after formation. Thus, a

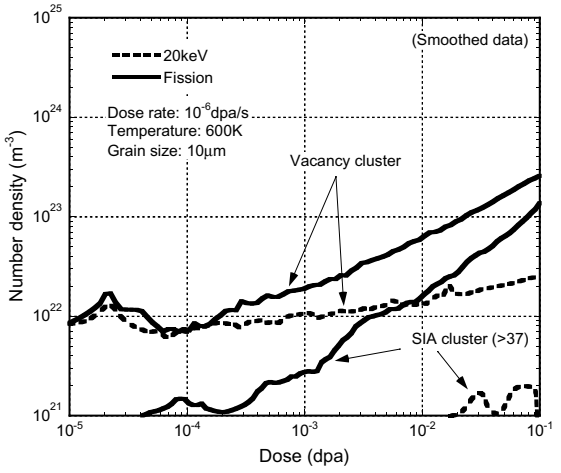

Fig. 10. Defect number densities irradiated with two different PKA spectra: (a) fission spectrum and (b) 20 keV spectrum. Defect accumulation by 20 keV irradiation is very small compared to that by fission irradiation. Slope of the line of vacancy cluster is very small, and almost no large SIA clusters are formed in this dose range.

large number of free vacancies are available, which enhance the growth of large vacancy clusters even though they are meta-stable situation, and also enhance the annihilation by recombine with SIAs to suppress the growth of SIA clusters.

Fig. 10 shows the effect of PKA spectrum, where defect number densities due to fission spectrum and 20 keV monotonic spectrum are compared at 600 K. The characteristics of the fission spectrum are given in Section 2.2. The defect number densities due to 20 keV spectrum is very small compared with the fission spectrum. The slope of vacancy number density is also small, and moreover, the formation of SIA clusters are significantly suppressed. Here we need to consider the effect of high PKA energy cascades in the fission spectrum. In the fission spectrum simulated using our MD cascade database, about one third of cascades have the PKA energy of 50 keV, and they differ from the other lower energy cascades in that they can produce very large SIA clusters by the mechanism of sub-cascade overlapping [11] whose chance is very small in 20 keV cascades. Therefore, our view is that SIA cluster formation is primarily owing to direct formation of large SIA clusters in high-energy displacement cascades. For the fusion spectrum, mean PKA energy will be less than 10 keV and the fraction of high-energy PKA cascades is smaller than the fission spectrum [13]. Similar results to 20 keV spectrum are expected for the fusion spectrum. However, it should be noted that in the fusion environment, the dose of interest is generally several orders of magnitude larger than that for reactor pressure vessels of fission reactors.

3.3. Vacancy jumps

Number of vacancy jumps should be a good measure to discuss a possible behavior of substitutional solute atoms that diffuse in the Fe matrix by a vacancy mechanism. Fig. 11 shows the total number of vacancy jumps in the computation cell of $100\times100\times100$ nm^3 cube as a function of dose for different dose rates. It is clear that the number of vacancy jumps at the fastest dose rate of 10^{-4} dpa/s differs from those at slower dose rates over the dose range of interest. This suggests that the solute diffusion at high dose rate is highly diminished resulting in less precipitation and segregation of solute atoms. The number of vacancy jumps at 10^{-6} dpa/s does not differ very much until high dose range in good correspondence with the effect of dose rate on the SIA cluster formation as shown in Fig. 8(b), where we can see at high doses an increase of the number density of the defect clusters, especially of SIA type, which act as strong sinks of vacancies. No dose rate effect is observed at the dose rates of 10^{-8} and 10^{-10} dpa/s. This means that the cascade annealing and subsequent long-range diffusion of vacancies complete well before the next displacement cascade occurs in the same area. In such cases, the number of vacancy jumps is determined simply from the geometrical configuration of vacancy sinks including those induced by irradiation and the resulting defect accumulation is not affected by dose rate.

Fig. 12(a) demonstrates the number of vacancy jumps as a function of dose rates. Dotted and dashed lines show the accumulated numbers of jumps of irradiation-induced vacancies and thermal vacancies, respectively, at a dose of 0.01 dpa. We estimated the number of thermal vacancy jumps using the following equation:

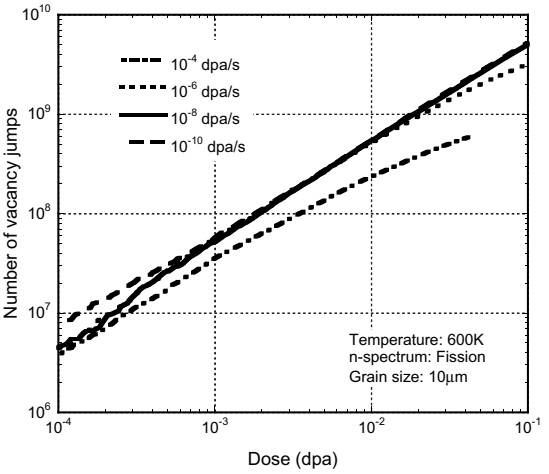

Fig. 11. Dose dependency of the number of jumps of irradiation-induced vacancies in the $100\times100\times100$ nm^3 computation box at different dose rates.

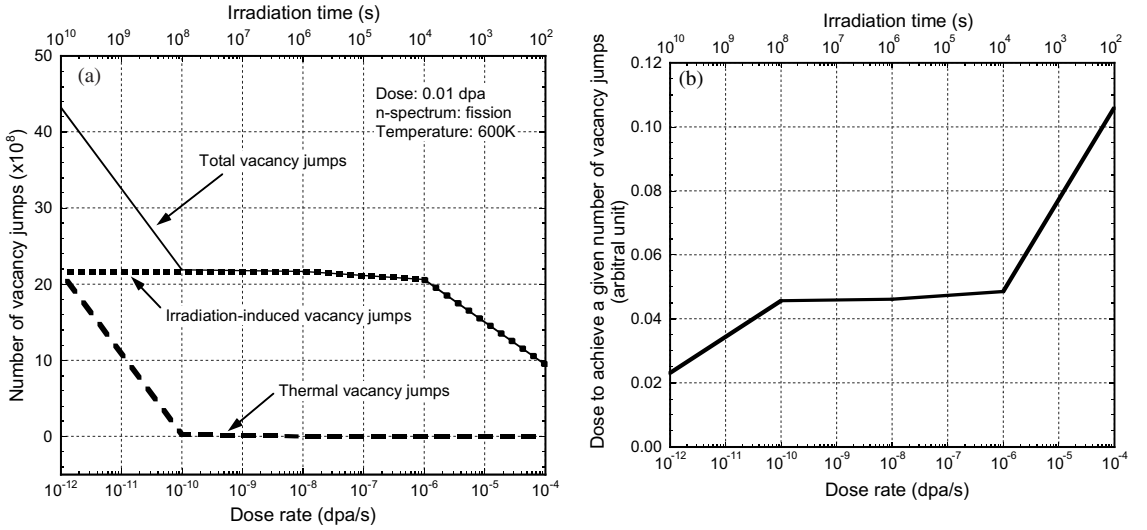

Fig. 12. Dose rate dependency of (a) the total number of vacancy jumps at 0.01 dpa, and (b) dose to achieve a given number of vacancy jumps. Both irradiation-induced vacancies and thermal vacancies are considered. Irradiation time is calculated from the dose divided by the dose rate. The solid line in (b) is an inverse of the solid line in (a).

$$n_{\mathrm{th}} = t \cdot \frac{6}{\delta^2} \cdot D_0 \cdot \exp\left(-\frac{E_{\mathrm{m}}^{\mathrm{v}}}{kT}\right) \cdot 2\left(\frac{\ell}{a_0}\right)^3 \cdot \exp\left(\frac{S_k}{k}\right) \cdot \exp\left(-\frac{E_{\mathrm{f}}^{\mathrm{v}}}{kT}\right), \quad (1)$$

where δ is the jump distance (0.248 nm), D_0 the pre-exponential factor of vacancy diffusion (10^{-2} cm^2 s^{-1}), $E_{\mathrm{m}}^{\mathrm{v}}$ the vacancy migration energy (1.2 eV), ℓ the edge length of computation cell cube (100 nm), a_0 the lattice constant (0.287 nm), $\exp\left(\frac{S_k}{k}\right)$ the entropy term ($\sim$10), $E_{\mathrm{f}}^{\mathrm{v}}$ the vacancy formation energy (1.73 eV), k the Boltzman's constant and T the irradiation temperature (600 K). The number of jumps of irradiation-induced vacancies is a function of dose rate at high dose rates of $>10^{-6}$ dpa/s, while it is independent of dose rates at lower dose rates. On the other hand, the number of thermal vacancy jumps looks dose rate dependent at very low dose rates. This happens because low dose rates require sufficiently long time to achieve a given dose of 0.01 dpa at low dose rates, and this long irradiation times allow for thermal vacancies to make more jumps than at higher dose rates. At high dose rates, the number of thermal vacancy jumps is negligible when compared with number of jumps of irradiation-induced vacancies. Fig. 12(a) shows that the numbers of jumps of irradiation-induced vacancies and thermal vacancies reach to a same magnitude at sufficiently low dose rates, where commercial reactor pressure vessels operate. The solid line of Fig. 12(a) is a sum of the jumps of irradiation-induced vacancies and thermal vacancies. It appears that there are two dose rate regions where the number of vacancy jumps is dose rate dependent, and there is a dose-rate independent area in between.

The inverse value of the number of jumps means a dose required to achieve a given number of vacancy jumps, and it is shown in Fig. 12(b). Since the number of vacancy jumps should be directly related to the diffusion of solute atoms of substitutional type, this line suggest that the solute precipitation/segregation is accelerated at lower dose rates, but it is independent of dose rate at intermediate dose rates (10^{-10}–10^{-6} dpa/s), and it is delayed at higher dose rates. The results well explain the proposed model on the copper precipitation in reactor pressure vessel materials by Odette et al. [23].

Of course these estimates change by non-trivial amount when we use different set of properties. Regarding the irradiation-induced vacancy jumps, a more appropriate value for the vacancy migration energy in real steels may be 1.2 eV, which considers the trap-limited long-range diffusion by carbon, as we did in the estimation of thermal vacancy jumps in pure iron rather than 0.5 eV. We are now doing additional KMC simulations using 1.2 eV for vacancy migration to estimate the effect of the migration energy on the number of jumps of irradiation-induced vacancies. The simulation is still on-going, but preliminary data show that the number of irradiation-induced vacancy jumps becomes dose rate dependent at dose rates higher than 10^{-8}–10^{-6} dpa/s for 1.2 eV migration energy, which is lower than the values of 10^{-6}–10^{-4} dpa/s for 0.5 eV migration energy. As expected, the total numbers of vacancy jumps at lower dose rates are not changed even when 1.2 eV migration energy is used. There should still be a certain amount of uncertainty in the present estimation. However, when we consider the accelerated embrittlement of copper containing reactor pressure vessel materials at

low dose rate [24], the result of present computer simulations seems to provide a reasonable explanation on the underlining mechanism of dose rate effect.

3.4. Defect annihilation at sinks

Finally the effect of defect sinks on defect annihilation is discussed. A new model of finite periodic boundary condition first allows us to estimate the effect of grain boundaries of realistic sizes at atomistic-level simulations. Fig. 13(a) and (b) show the effect of grain size on the number densities of vacancy clusters and SIA clusters, respectively. Grain sizes considered range from 1 to 100 μm. The effect of grain size is not very large and looks saturated for the grain sizes of 10 and 100 μm, which are realistic sizes for real steels. Point sinks are also included simultaneously to simulate pre-existing dislocations. Fractions of defect annihilation at grain boundaries are ~10%, ~1% and ~0.1% for grain sizes of 1, 10 and 100 μm, respectively, and this data on fraction will support the saturation effect of grain boundary size. Smallest grain size of 1 μm gives larger number density of vacancy clusters and smaller number density of SIA clusters. This is explained as that the fast one-dimensional motion of SIA clusters removes SIA clusters at grain boundaries very easily when the grain size is as small as 1 μm, and excess amount of vacancies which are to annihilate by recombination with SIA clusters are left behind.

Fig. 14(a) and (b) show the comparison of the number of annihilations of vacancies and SIAs at (a) grain boundaries and (b) dislocations at the dose of 0.01 dpa. The amount of SIA annihilation at grain boundaries is about three times larger than that of vacancy annihilation presumably due to long range one-dimensional motion of SIA clusters as expected. Defect annihilation is independent of the dose rate in the range from 10^{-10} to 10^{-6} dpa/s, but at the highest dose rate of 10^{-4} dpa/s, annihilation of SIAs is almost halved while that of vacancies is reduced by about 20%. High dose rate terminates the long-range migration of SIA clusters. At the lower temperature of 350 K, absolute number of annihilations decreases due to less mobility of defects and high number density of defect clusters as shown in Fig. 2. However, it is interesting to see that the ratio of vacancy and SIA annihilations at grain boundaries is again about three. It should be noted that the situation may change at higher doses.

On the other hand, regarding the annihilation at dislocations, the numbers of vacancy and SIA annihilations are almost the same at the dose rates ranging from 10^{-6} to 10^{-10} dpa/s at 600 K. The absolute values of the number of annihilations at dislocations are almost 30 times larger than those at grain boundaries. Since the cross-section of the reaction between SIA clusters and point dislocations should not be very large due to one-dimensional motion of the SIA clusters, the simulation results suggest that long-range migration of SIA clusters before reaching at grain boundaries earn the amount of reactions. At the high dose rate of 10^{-4} dpa/s, increase in defect concentration decreases the amount of annihilations at dislocations. However, the effect of dose rate is different for vacancies and SIAs. For vacancies, the cross-section is three-dimensional because of the three-dimensional motion of mobile vacancies. However, for the SIA clusters, the cross-section is two-dimensional because the concern for a SIA cluster is if there exist any defects on the one-dimensional migration line. This difference in the nature of the reaction cross-section results in the difference at the higher dose rate. At the low

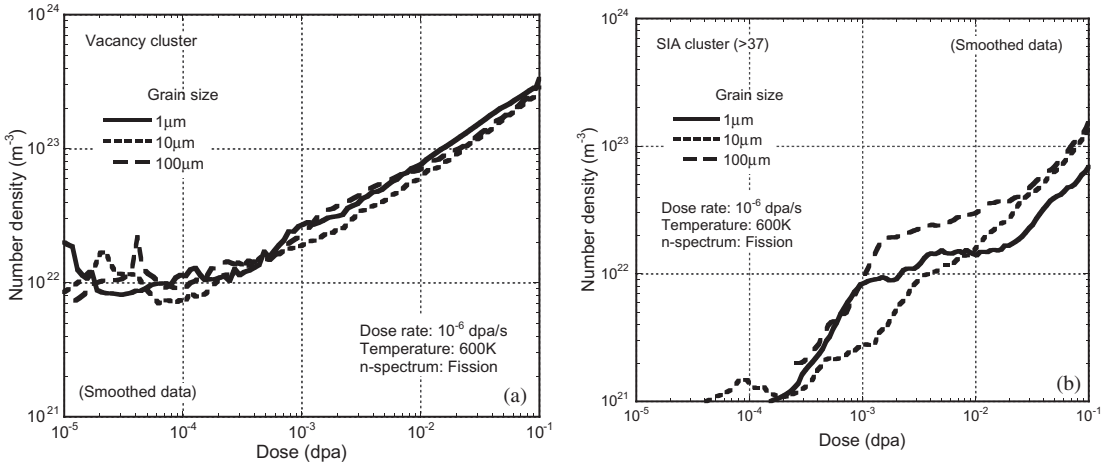

Fig. 13. Effect of grain size on (a) vacancy cluster and (b) SIA cluster formation. The calculated data are smoothed to clarify the difference among the results.

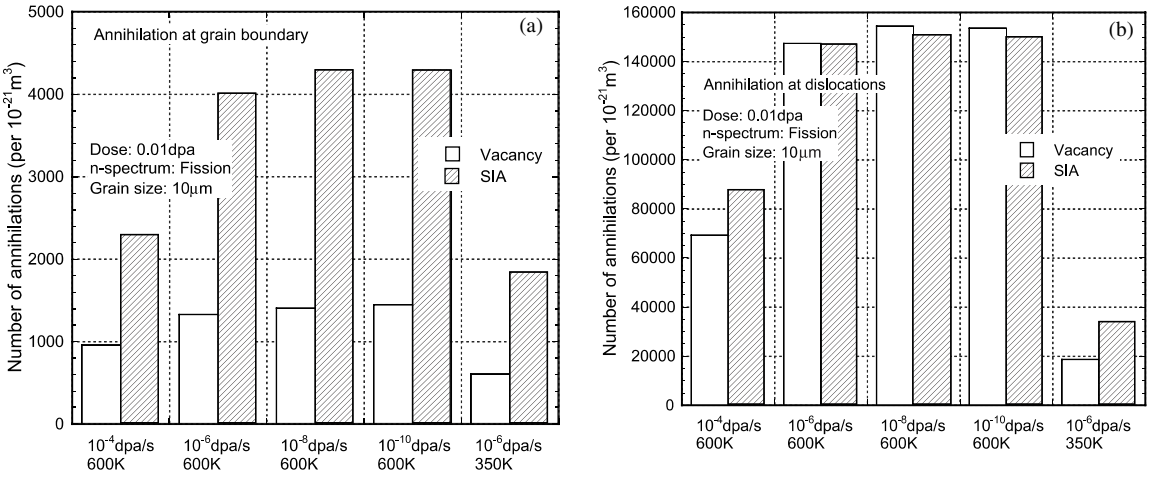

Fig. 14. Number of point defect annihilations at (a) grain boundaries and (b) dislocations at the dose of 0.01 dpa.

temperature of 350 K, the annihilation at dislocations reduces significantly. We assume that the same mechanism as dose rate effect is effective for the lower irradiation temperature conditions. Again we need to be careful that the dose level may change the situation.

4. Summary

Kinetic Monte Carlo computer simulations on the defect accumulation in neutron-irradiated bcc-Fe are presented. We propose a comprehensive KMC model to simulate the irradiation response of bcc-Fe under neutron irradiation together with a new periodic boundary condition to consider grain boundaries. Comparisons of the KMC simulations with the recent experiments demonstrate the validity of the proposed KMC model.

Then, the effect of irradiation temperature, dose rate, and neutron spectrum are studies using this technique. The effect of temperature is very significant. The high temperature irradiation in the temperature range of the stage V allows for vacancy clusters to grow, but the growth of SIA clusters at 600 K is suppressed compared with the results at 350 K. The magnitude of dose rate effect is irradiation-temperature dependent. At low temperature irradiation of 350 K, the dose rate effect is not very large, but it is at high temperature of 600 K. Existence of a threshold dose rate is confirmed for the dose rate effect on defect production at 600 K. Below this threshold dose rate, no stable vacancy clusters are formed, and the formation of SIA clusters are dose rate independent.

A new quantitative evaluation of the number of vacancy jumps is performed to investigate the possibility of the effect of irradiation variables on the solute diffusion by vacancy mechanism in bcc-Fe. The results show that the total number of vacancy jumps is dose rate dependent at low dose rates below 10^{-10} dpa/s and at higher dose rates above 10^{-6} dpa/s in pure bcc-Fe. However the nature of the dose rate effect at low dose rates are essentially thermal aging, while the dose rate effect at high dose rates is the intercascade interaction. It should be noted that the threshold values of the dose rate effects depends on the mobility of the vacancies. Finally the effect of defect sinks such as grain boundaries and dislocations are discussed.

Acknowledgements

The authors would like to thank Dr M.J. Caturla of University of Alicante for her fruitful discussions on the KMC simulations. The authors would also like to thank Professor M. Hasegawa of Tohoku University for his advice in interpreting experimental data.

References

[1] G.R. Odette, G.E. Lucas, Radiat. Eff. Def. Solids 144 (1998) 189.
[2] For example S. Takaki, J. Fuss, H. Kugler, U. Dedek, H. Schultz, Radiat. Eff. 79 (1983) 87;
A. Vehanen, P. Hautojarvi, J. Johansson, J. Yli-Kauppila, Phys. Rev. B 25 (1982) 763.
[3] For example M.L. Jenkins, C.A. English, B.L. Eyre, Philos. Mag. A 38 (1978) 97;
M.A. Kirk, I.M. Robertson, J.L. Jenkins, C.A. English, T.J. Black, J.S. Vetrano, J. Nucl. Mater. 206 (1987) 21.
[4] Example of early work is B.L. Eyre, A.F. Bartlett, Philos. Mag. 12 (1965) 261, Most recent works can be found in Refs. [20,21].
[5] T. Diaz de la Rubia, A. Rev. Mater. Sci. 26 (1996) 613.

[6] Yu.N. Osetsky, D.J. Bacon, A. Serra, B.N. Singh, S.I. Golubov, Philos. Mag. 83 (2003) 61.
[7] H.L. Heinisch, B.N. Singh, J. Nucl. Mater. 232 (1996) 206.
[8] M. Jaraiz, G.H. Gilmer, J.M. Poate, T. Diaz de la Rubia, Appl. Phys. Lett. 68 (1996) 409.
[9] M.J. Caturla, N. Soneda, E. Alonso, B.D. Wirth, T. Diaz de la Rubia, J.M. Perlado, J. Nucl. Mater. 276 (2000) 13.
[10] N. Soneda, T. Diaz de la Rubia, Philos. Mag. A 78 (1998) 995.
[11] N. Soneda, S. Ishino, T. Diaz de la Rubia, Philos. Mag. Lett. 81 (2001) 649.
[12] N. Soneda, S. Ishino, T. Diaz de la Rubia, unpublished work.
[13] L.R. Greenwood, J. Nucl. Mater. 216 (1994) 29.
[14] N. Soneda, T. Diaz de la Rubia, Philos. Mag. A 81 (2001) 331.
[15] Yu.N. Osetsky, D.J. Bacon, A. Serra, B.N. Singh, S.I. Golubov, Philos. Mag. 83 (2003) 61.
[16] B.D. Wirth, G.R. Odette, D. Maroudas, G.E. Lucas, J. Nucl. Mater. 276 (2000) 33.
[17] T. Tabata, H. Fujita, H. Ishii, K. Igaki, M. Ishiki, Scr. Metal. 15 (1981) 1317.
[18] A. Takahashi, N. Soneda, S. Ishino, unpublished work.
[19] M. Eldrup, B.N. Singh, S.J. Zinkle, T.S. Gyun, K. Farrell, J. Nucl. Mater. 307–311 (2002) 912.
[20] M.L. Jenkins, M.A. Kirk, Characterization of Radiation Damage by Transmission Electron Microscopy, Institute of Physics Publishing, Bristol and Philadelphia, 2001.
[21] M. Victoria, N. Baluc, C. Bailat, Y. Dai, M.I. Luppo, R. Shaublin, B.N. Singh, J. Nucl. Mater. 276 (2000) 114.
[22] A.C. Nicol, M.L. Jenkins, M.A. Kirk, Mater. Res. Soc. Symp. Proc. 6500 (2001) R1.3.1.
[23] G.R. Odette, G.E. Lucas, D. Klingensmith, in: R.K. Nanstad, M.L. Hamilton, F.A. Garner, A.S. Kumar (Eds.), Effects of Radiation on Materials: 18th International Symposium, ASTM-STP-1325, ASTM, Philadelphia, PA, 1997, p. 88.
[24] Conference Proceedings of 'Workshop on dose rate effects in reactor pressure vessel materials,' EPRI 1006981, CRIEPI T980203, 12–14 November 2002, Olympic Valley, CA.